On the reduction of quasi-cyclic disk models with variable rotation speeds

Arnaud Sternchuss, Etienne Balmes
Ecole Centrale Paris, Laboratoire MSS-MAT,
Grande Voie des Vignes, 92295 CHATENAY-MALABRY, France
e-mail: **arnaud.sternchuss@ecp.fr**

Abstract

New methods for the dynamic analysis of tuned and mistuned bladed disks are presented. A new technique for disk substructuring using parameterized superelements is first described. It allows individual blade mistuning to be taken into account as slight variations in the reduced stiffness matrix of the bladed sectors or as shifts in fixed blade frequencies. A parametric multi-model reduction approach is then introduced to allow predictions of the evolution of vibration characteristics with respect to the rotation speed. Using prestressed solutions at three rotations speeds, this method allows a very accurate reanalysis of modes and forced responses of mistuned disks at all intermediate speeds.

1 Introduction

This work deals with the parametric reduction of models of structures whose nominal configuration presents properties of cyclic symmetry. The objective is to build a reduced model that represents particular mode-shapes exactly and others with a good accuracy for variable rotation speeds and mistuning levels. In a recent survey, Castanier and Pierre [1] review the latest advances in the field of the vibration of bladed disks and underline some new directions of research for the study of mistuning and rotation.

Section 2 summarizes the mechanical problem related to rotating structures with a focus on those who present properties of cyclic symmetry and to which a specific substructuring technique can be applied. This property vanishes when material or geometrical differences occur from blade to blade. This phenomenon called mistuning is mainly due to manufacturing process or service wear. It is often modeled as a random phenomenon which requires a statistical approach through Monte-Carlo simulations. But where cyclic symmetry considerations can be used to model tuned disks, mistuned disks should be modeled fully since each sector is different. This is not acceptable in many instances. Many reduction techniques have thus been introduced. They often include methods derived from the tuned system analysis coupled with either a CMS method [2–6] or a non-CMS method [3, 7–9], assuming in every case that mistuned modes are given by projecting the individual blade mistuning onto the tuned system modes. In the case of large mistuning, the non CMS technique has been improved by building a reduction basis made of tuned system normal modes and blade static or quasi-static modes [10]. The quasi-cyclic reduction technique presented here uses a physical description of the bladed disk motion to build accurate reduced disk models with parameterized superelements. Small blade mistuning is easily taken into account as slight shifts in the natural frequencies of the bladed sector with fixed interfaces or directly as variations of the reduced stiffness matrix. Computations of the modal characteristics of the tuned or mistuned assembly of superelements are then really straight forward.

Among the other emerging computational challenges is the influence of the inertial effects induced by rotation. To address this issue a modal analysis technique has been proposed by Marugabandhu and Griffin [11] that consists in seeking the modes at any rotation speed as a linear combination of modes at rest. Section 4 presents a multi-model reduction approach [12] that can be applied to build full Campbell diagrams of tuned

or mistuned structures using exact computations of targeted modes at selected rotation speeds. As an illustration the Campbell diagram of a tuned disk is built through this method. The multi-model reduction basis itself can be then built through the quasi-cyclic reduction technique which results in very fast computations of the modes and the response of the disk in either tuned or mistuned cases.

2 Mechanical problem associated with a rotating structure

The disk presented in figure 1 is supposed to be in rotation with the angular speed Ω. The full mesh of the disk is composed of 20 node hexahedrons and 15 node pentahedrons with a total of $N = 293457$ DOFs. The front and aft rims are fixed. The material is titanium. In the following, for confidentiality reasons, all frequencies are normalized with respect to the lowest tuned frequency.

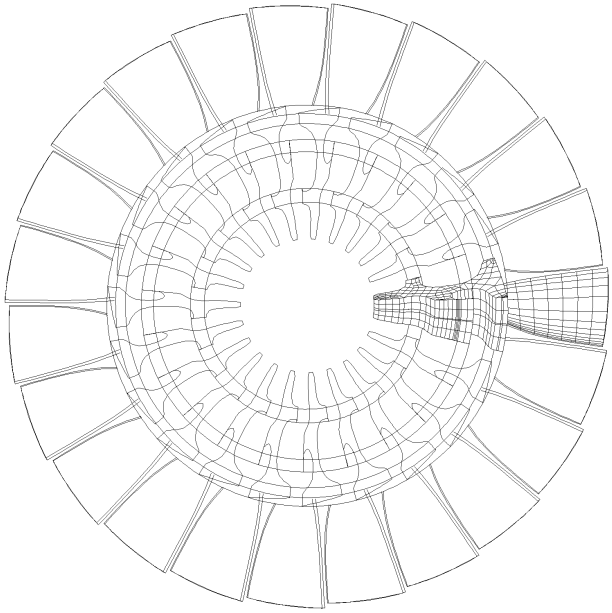

Figure 1: Sample disk

2.1 Rotation induced effects

The discrete dynamic problem is written in the frequency domain under the general form

$$[Z(\omega,\Omega)]_{N\times N}\{q(\Omega)\}_{N\times 1} = \{f(\omega,\Omega)\}_{N\times 1} \tag{1}$$

where $\{q(\Omega)\}$ stands for the DOFs vector of the disk, $\{f(\omega,\Omega)\}$ for the applied load and $[Z(\omega,\Omega)]$ for the dynamic stiffness, including the effects induced by the rotation speed Ω

$$[Z(\omega,\Omega)] = -\omega^2\,[M] + i\,\omega\,[C(\omega,\Omega)] + [K(\omega,\Omega)] \tag{2}$$

with:

- $[M]$ the mass matrix;
- $[C(\omega,\Omega)] = [D(\omega)] + [C_g(\Omega)]$ the viscous matrix, with $[D(\omega)]$ the damping matrix and $[C_g(\Omega)]$ the gyroscopic coupling;

- $[K(\omega,\Omega)] = [K_{NL}(\omega,\Omega)] + [K_g(\Omega)] + [K_a(\Omega)]$ the stiffness matrix, with $[K_{NL}(\omega,\Omega)]$ the nonlinear tangent stiffness matrix stating that the disk vibrates around a prestressed state induced by inertia loading, $[K_g(\Omega)]$ the gyroscopic stiffness and $[K_a(\Omega)]$ the centrifugal acceleration.

Here Ω will be assumed constant so that the matrix $[K_a(\Omega)]$ which depends only on $\dot{\Omega}$ is equal to zero. Notice that $[C(\omega,\Omega)]$ and $[K_{NL}(\omega,\Omega)]$ can depend both on frequency, for viscoelastic materials [13], and on rotation speed. In the following one assumes that neither the damping nor the stiffness matrix depend on frequency. To simplify further notations the dependance of $[Z]$, $\{q\}$ and $\{f\}$ on ω and/or Ω will be explicited only if needed.

The general form of problem (1) implies that the determination of free vibration modes or the computation of the forced response of a structure including rotation effects is performed through two steps:

- the static response of the structure under the inertial load associated with a constant rotation speed is computed;
- the response of the structure prestressed by the initial load is obtained using the tangent stiffness matrix associated with the static stress state.

The true static computation should consider large deformation effects and the nonlinear characteristics of inertia forces which are follower forces, i.e. they depend of the current state of deformation. In this paper, one will however assume, as acceptable in many industrial applications, that a linear computation of the inertial load is sufficient. This results in

$$\{f(\Omega)\} = \Omega^2 \{f^1\} = \Omega^2 \int_{disk} \rho\, r(\Omega = 0)\, dV \tag{3}$$

and one assumes that the static displacement is solution of the linear problem

$$[K(\Omega = 0)]_{N\times N}\{q_{stat}\}_{N\times 1} = \Omega^2 \{f^1\}_{N\times 1} \tag{4}$$

where it is apparent that $\{q_{stat}\}$ is directly proportional to Ω^2. In the nonlinear tangent stiffness the deformation induced by $\{q_{stat}\}$ appears quadratically, it results that the tangent stiffness is a second order matrix polynomial in Ω^2. Similarly the gyroscopic stiffness is clearly proportional to Ω^2. One can finally write

$$[Z(\omega,\Omega)] = -\omega^2[M] + i\,\omega\,[C] + \sum_{p=0}^{2} \Omega^{2p}\,[K^p] \tag{5}$$

Recall that the stiffness matrix depends only on Ω due to the fact that in this study one only considers elastic materials. Computations are simplified by the fact that only five constant matrices are needed whatever the rotation speed. If the range of rotation speed is $[0, \Omega_{max}]$, these constant matrices are given by

$$\begin{aligned}
&[M]_{N\times N}\\
&[C]_{N\times N}\\
&\big[K^0\big]_{N\times N} = [K(0)]\\
&\big[K^1\big]_{N\times N} = \frac{1}{3\Omega_{max}^2}\left(16\big[K(\tfrac{1}{2}\Omega_{max})\big] - [K(\Omega_{max})] - 15[K(0)]\right)\\
&\big[K^2\big]_{N\times N} = \frac{4}{3\Omega_{max}^4}\left([K(\Omega_{max})] - 4\big[K(\tfrac{1}{2}\Omega_{max})\big] + 3[K(0)]\right)
\end{aligned} \tag{6}$$

Notice that the elastic stiffness of the structure appears directly in the matrix polynomial as the term $\big[K^0\big]$.

2.2 Cyclic Symmetry

Structures that present cyclic symmetry are composed of N_s identical sectors, numbered from 0 to $N_s - 1$, generated by rotations of angle $\alpha = 2\pi/N_s$ around axis $O\mathbf{e_z}$ of a reference sector such as that of figure 1. In the following θ stands for the rotation of angle α around axis $O\mathbf{e_z}$. Since the model geometry is invariant by any rotation θ^s, it is useful to consider the displacement as a Discrete Fourier Series as proposed in [14]

$$\forall s \in \mathbb{N}_{N_s-1},\, \mathbf{u}(\mathbf{x^s}) = \sum_{\delta=\mathbf{0}}^{\mathbf{N_s/2}} \theta^{\mathbf{s}} \left(\mathbf{u}^{\delta}(\mathbf{x^0})\right) \mathbf{e}^{\mathbf{i}\,\mathbf{s}\,\delta\,\alpha} \tag{7}$$

The well known property of symmetry for DFT gives $\mathbf{u}^{\delta} = \overline{\mathbf{u}^{\mathbf{N_s}-\delta}}$ where $\overline{\mathbf{z}}$ denotes the complex conjugate. Given this relation, the number of independant harmonics is equal to $N_s/2$ if N_s is even and $(N_s-1)/2$ if N_s is odd. In particular, the eigenmodes come by complex conjugate pairs, except those with $\delta = 0$ and $\delta = N_s/2$ if N_s is even, which are real. In the limiting case of a structure invariant by any rotation (pure axisymmetry), N_s goes to infinity and (7) becomes a Fourier Series.

The angular harmonic δ has various denominations: "Fourier/Floquet coefficient", "interblade/intersector phase index", "circumferential wave number"... All these denominations are equivalent since $\delta\,\alpha$ is a wave number that represents the phase difference between two adjacent sectors. As a result, if $\delta\,\alpha \equiv 0\,[2\pi]$ these sectors vibrate in phase whereas if $\delta\,\alpha \equiv \pi\,[2\pi]$ they vibrate in antiphase. In the latter case this implies that the motion of the interface between two sectors is null for compatibility with the antiphase condition. The motion of the bladed disk is thus very close to that of the sectors with their interfaces fixed. If one considers the circumferential modeshapes, δ corresponds to their number of nodal diameters. The Fourier coefficients $\mathbf{u}^{\delta}$ are classically defined on the first sector (coordinates $\mathbf{x^0}$). Nevertheless, they could be propagated to other sectors with

$$\forall s \in \mathbb{N}_{N_s-1},\, \mathbf{u}^{\delta}(\mathbf{x^s}) = \theta^{\mathbf{s}} \left(\mathbf{u}^{\delta}(\mathbf{x^0})\right) \mathbf{e}^{\mathbf{i}\,\mathbf{s}\,\delta\,\alpha} \tag{8}$$

It can be shown from finite groups theory [15] of Floquet's theory [16] that eigenmodes only involve a single harmonic δ. In most practical cases, the external load is decomposed using the same Fourier strategy and the forced responses associated with each "engine order", i.e. each load harmonic, are computed. This is due to the fact that a perfectly tuned disk will respond only on the angular harmonics equal to those of the external load [17, 18].

While (7) and (8) relate Fourier harmonics on the nominal sector and motion on the full disk, it does not account for the continuity of displacement between sectors. As shown in figure 2, one considers two matching right and left surfaces $\mathcal{I}_r^s$ and $\mathcal{I}_l^s$ and an interior domain $\mathcal{D}_c^s$. The right and left surfaces are matching in the sense that for any point $\mathbf{x_r^s}$ on $\mathcal{I}_r^s$, $\mathbf{x_l^s} = \theta(\mathbf{x_r^s})$ is on $\mathcal{I}_l^s$.

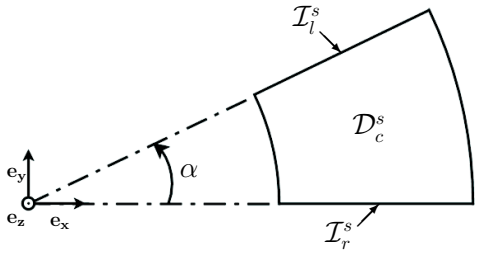

Figure 2: Subdomains of sector s

Intersector continuity between sectors s and $s+1$ is simply given by

$$\begin{aligned} &\forall s \in \mathbb{N}_{N_s-1}, \forall \mathbf{x_l^s} \in \mathcal{I}_\mathbf{l}^\mathbf{s}, \exists \mathbf{x_r^{s+1}} \in \mathcal{I}_\mathbf{r}^{\mathbf{s+1}}, \\ &\mathbf{x_l^s} = \mathbf{x_r^{s+1}} \text{ and } \mathbf{u}(\mathbf{x_l^s}) = \mathbf{u}(\mathbf{x_r^{s+1}}) \end{aligned} \tag{9}$$

For both compatible and incompatible meshes, continuity conditions of the form (9) can be written as a set of linear constraints associated with interface DOFs [19]. One thus defines right and left observation equations

which for compatible meshes give a discrete representation of the motion $\mathbf{u}(\mathbf{x_l^s})$ on the left interface $\mathcal{I}_l^s$ and the rotation θ of the corresponding motion on the right interface $\mathcal{I}_r^s$.

$$\begin{aligned} \theta\left(\mathbf{u}(\mathbf{x_r^s})\right) &\Longrightarrow \{q_r^s\} = [c_r]\{q^s\} \\ \mathbf{u}(\mathbf{x_l^s}) &\Longrightarrow \{q_l^s\} = [c_l]\{q^s\} \end{aligned} \tag{10}$$

$\{q^s\}$ is the DOFs vector on sector $\mathcal{D}^s$. Notice that $[c_r]$ takes the rotation θ into account so that the displacement is expressed in a basis coherent with the interface motion. If the mesh at interfaces is regular, the observation matrices are identical for all sectors.

In the tuned case, displacements of particular interest are those who involve a single harmonic δ. With the assumption of cyclic symmetry, problem (1) can be restrained to a single sector

$$[Z^s]_{N^s \times N^s}\{q^s\}_{N^s \times 1} = \{f^s\}_{N^s \times 1} \tag{11}$$

where $[Z^s]$ has the same properties as described in section 2.1. However, an additional constraint equation has to be introduced to take the continuity condition between sectors into account. Substituting equation (9) into equation (8) gives

$$\begin{aligned} &\forall s \in \mathbb{N}_{N_s-1}, \forall \mathbf{x_l^s} \in \mathcal{I}_\mathbf{l}^\mathbf{s}, \exists \mathbf{x_r^s} \in \mathcal{I}_\mathbf{r}^\mathbf{s}, \\ &\mathbf{x_l^s} = \theta(\mathbf{x_r^s}) \text{ and } \mathbf{u}^\delta(\mathbf{x_l^s}) = \theta\left(\mathbf{u}^\delta(\mathbf{x_r^s})\right) \mathbf{e}^{\mathbf{i}\,\delta\,\alpha} \end{aligned} \tag{12}$$

which, when discretized, leads to a constraint equation of the form

$$\left([c_l] - e^{i\,\delta\,\alpha}\,[c_r]\right)\ (\Re\{q^s\} + i\Im\{q^s\}) = \{0\} \tag{13}$$

Since $e^{i\,\delta\,\alpha} = \cos(\delta\,\alpha) + i\sin(\delta\,\alpha)$, one often considers a double sector approach separating the real and imaginary parts

$$[c_\Re(\delta)]\left\{ \begin{array}{c} \Re\{q^s\} \\ \Im\{q^s\} \end{array} \right\} = \{0\} \tag{14}$$

with

$$[c_\Re(\delta)] = \left[\begin{array}{cc} [c_l] - \cos(\delta\,\alpha)[c_r] & \sin(\delta\,\alpha)[c_r] \\ -\sin(\delta\,\alpha)[c_r] & [c_l] - \cos(\delta\,\alpha)[c_r] \end{array} \right]_{2N_r \times 2N} \tag{15}$$

Recall that $\Im\{q^s\} = \{0\}$ for $\delta = 0$ and $\delta = N_s/2$ if N_s is even, in this case the double sector approach is equivalent to a single sector approach with a simple continuity condition between two adjacent sectors. The solutions are then sought in the kernel of $[c_\Re(\delta)]$ by projecting problem (11) onto the basis of this kernel denoted $[T_{Ker}(\delta)]$.

3 Quasi-cyclic reduced models

As actual disks are not perfectly periodic due to manufacturing tolerances and service wear, extensive computations using statistical approaches such as Monte-Carlo simulations are widely used. These blade to blade differences called mistuning also imply that the full problem (1) has to be assembled then solved. Because of the actual size of the finite element models used in industry, typically around one million DOFs, there is a great need for reduced order models. In the proposed quasi-cyclic (QC) reduction technique one builds individual sector superelements that:

- allow parametrization of the sector in rotation and mistuning described as slight deviations of its natural frequencies when its interfaces are fixed,
- reproduce exact results in certain configurations;
- can be assembled into a disk model.

3.1 Basis of modes

To allow assembly into a disk model the proposed method combines matching left and right interface modes and interior modes for which the interfaces are fixed, as illustrated in figure 3.

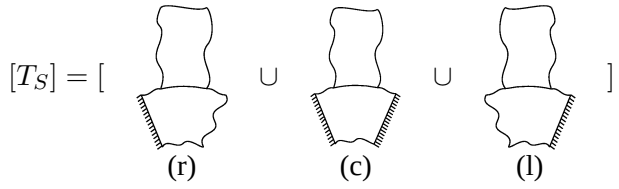

Figure 3: Reduction basis

The reduced sector model thus distinguishes right, complementary and left generalized DOFs for sector s

$$[Z_S^s(\omega,\Omega)]_{N_S^s \times N_S^s} \left\{ \begin{array}{c} q_{Sr}^s \\ q_{Sc}^s \\ q_{Sl}^s \end{array} \right\}_{N_S^s \times 1} = \left\{ \begin{array}{c} f_{Sr}^s \\ f_{Sc}^s \\ f_{Sl}^s \end{array} \right\}_{N_S^s \times 1} \tag{16}$$

which are related to initial sector DOFs by a constant basis $[T_S]$ with

$$\{q^s\}_{N^s \times 1} = \left[\begin{array}{ccc} [T_{Sr}] & [T_{Sc}] & [T_{Sl}] \end{array} \right]_{N^s \times N_S^s} \left\{ \begin{array}{c} q_{Sr}^s \\ q_{Sc}^s \\ q_{Sl}^s \end{array} \right\}_{N_S^s \times 1} \tag{17}$$

The first step of the proposed procedure is to build the subspace generated on sector 0 by the target modes, i.e. selected modes that will be found exactly by solving the reduced problem. These modes are selected with respect to the characteristics of the tuned motion that depends on δ:

- a set of tuned eigenmodes $[\Phi_{tun}]$ with low values of δ to account for the disk-dominated motion computed using cyclic symmetry methods presented in section 2.2 and thus identical for all sectors;
- a set of modes of sector with fixed interfaces $[\Phi_{fix}]$ to account for the blade-dominated motion.

This basis is built through the following procedure:

- Most of the cyclic eigenmodes are complex and their real and imaginary parts are first separated

$$[T_b]_{N \times N_b} = \left[\begin{array}{ccc} \Re([\Phi_{tun}]) & \Im([\Phi_{tun}]) & [\Phi_{fix}] \end{array} \right] \tag{18}$$

- One considers only the restriction of the modes of the entire structure on both interfaces

$$[T_{rl}]_{(N_r+N_l)\times N_{rl}} = \left[\begin{array}{c} [c_r][T_b] \\ [c_l][T_b] \end{array} \right] \tag{19}$$

  Fixed interface modes vanish naturally at this step. A Singular Value Decomposition (SVD) of $[T_{rl}]$ is performed

$$[T_{rl}] = [U][\Sigma][V] \tag{20}$$

  $[\Sigma]$ is the matrix of the singular values λ_j. N_λ is then defined by

$$N_\lambda = max\{j, \lambda_j/\lambda_1 > \varepsilon\} \tag{21}$$

where ε is chosen to keep a sufficient independence between interface and interior modes.

According to the properties of SVD, the β first columns of U, $(\{u_1\},\ldots,\{u_\beta\})$, are a basis of the image of $[T_{rl}]$. Therefore, this leads to a basis of modes restricted to the interface. Then, from basis $[T_b]$, one defines

$$\begin{aligned}[T_c] &= \left[\begin{array}{cc} [T_b][v_j]_{j>N_\lambda} & [\Phi_{fix}] \end{array}\right] \\ [T_i] &= [T_b][v_j]_{j\leq N_\lambda}\end{aligned} \tag{22}$$

$[T_c]$ contains both the eigenmodes rejected by the SVD and the initial modes with fixed interfaces. An additional zero condition is imposed at the interfaces in the first equation to ensure that $[T_c]$ will really be a basis for interior modes with both interfaces fixed, that is to say a basis for modes that correspond to diagram (c) of figure 3

$$[T_c]_{|\mathcal{I}_r\cup\mathcal{I}_l} = [0] \tag{23}$$

$[T_i]$ and $[T_c]$ are orthonormalized with respect to the elastic stiffness $\left[K^{0,0}\right]$ of sector 0 through a Gramm-Schmidt procedure:

$$[T_i] = [T_i] - \left[T_c^\top\ K^{0,0}\ T_c\right]^{-1}[T_c]\left[T_c^\top\ K^{0,0}\ T_i\right] \tag{24}$$

This leads to bases whose general forms are

$$[T_c]_{N\times(N_{rl}-N_\lambda)} = \left[\begin{array}{c}[0]\\ [T_{cc}]\\ [0]\end{array}\right] \text{ and } [T_i]_{N\times N_\lambda} = \left[\begin{array}{c}[T_{ir}]\\ [T_{ic}]\\ [T_{il}]\end{array}\right] \tag{25}$$

- the following step is to build the interface modes from $[T_i]$. This set of modes is completed such that

$$[T_i]_{N\ \times\ 2N_\lambda} = \left[\begin{array}{cc}[T_{i1}] & [T_{i2}]\end{array}\right] \tag{26}$$

with

$$[T_{i1}] = \left[\begin{array}{c}[T_{ir}]\\ [T_{ic}]\\ [T_{il}]\end{array}\right] \text{ and } [T_{i2}] = \left[\begin{array}{c}[T_{ir}]\\ -\left[K_{cc}^{0,0}\right]^{-1}\left[K_{cr}^{0,0}\right][T_{ir}]\\ [0]\end{array}\right] \tag{27}$$

$[T_{i2}]$ contains the right interface modes, their static recovery on the complementary domain and no motion on the left interface.

- As stated before right and left interface modes are matched modulo θ. Introducing the following matrix

$$[B]_{2N_\lambda\ \times\ 2N_\lambda} = \left[\begin{array}{cc}[0] & [I]\\ \left([c_r]\left[\hat{T}^2\right]\right)^{-1}\left([c_l]\left[\hat{T}^1\right]\right) & -[I]\end{array}\right] \tag{28}$$

one builds

$$\left[\begin{array}{cc}[T_{Sr}] & [T_{Sl}]\end{array}\right]_{N\ \times\ 2N_\lambda} = [T_i][B] \tag{29}$$

with

$$\begin{aligned}[T_{Sr}]_{N\ \times\ N_\lambda} &= \left[\begin{array}{c}\theta\left([T_{il}]\right)\\ -\left[K_{cc}^{0,0}\right]^{-1}\left[K_{cr}^{0,0}\right]\theta\left([T_{il}]\right)\\ [0]\end{array}\right] \\ [T_{Sl}]_{N\ \times\ N_\lambda} &= \left[\begin{array}{c}[0]\\ [T_{ic}] + \left[K_{cc}^{0,0}\right]^{-1}\left[K_{cr}^{0,0}\right]\theta\left([T_{il}]\right)\\ [T_{il}]\end{array}\right]\end{aligned} \tag{30}$$

- With $[T_{Sc}] = [T_c]$ the basis is finally

$$[T_S] = \left[\begin{array}{ccc} [T_{Sr}] & [T_{Sc}] & [T_{Sl}] \end{array} \right] \tag{31}$$

This basis has the particular shape described by figure 3. $[T_{Sr}]$ is a basis of modes with right interface free and left interface fixed. $[T_{Sc}]$ is a basis of interior modes with both interfaces fixed. $[T_{Sl}]$ is a basis of modes with left interface free and right interface fixed.

3.2 Reduced matrices

Problem (11) is projected onto the constant reduction basis $[T_S]$ for each sector s. $[Z^s]$ is projected such that

$$[Z_S^s(\omega, \Omega)] = -\omega^2 \, [M_S^s] + i\,\omega \, [C_S^s] + \sum_{p=0}^{2} \Omega^{2p} \, \left[K_S^{s,p}\right] \tag{32}$$

where $[M_S^s] = \left[T_S^\top \, M^s \, T_S\right]$, $[C_S^s] = \left[T_S^\top \, C^s \, T_S\right]$ and $\left[K_S^{s,p}\right] = \left[T_S^\top \, K^{s,p} \, T_S\right]$, $p \in \{0, 2\}$.
Recall that $\left[K^{s,0}\right]$ is the elastic stiffness of sector s and this leads to the following relations

$$\begin{aligned} \left[T_{Sc}^\top \, M^s \, T_{Sc}\right] &= [I] \\ \left[T_{Sc}^\top \, K^{s,0} \, T_{Sr}\right] &= \left[T_{Sc}^\top \, K^{s,0} \, T_{Sl}\right] = [0] \\ \left[T_{Sc}^\top \, K^{s,0} \, T_{Sc}\right] &= [\mathcal{K}_{Sc}^s] = \left[\begin{array}{c} \backslash \\ \left(\omega_{cj}^s\right)^2 \\ \backslash \end{array} \right] \end{aligned} \tag{33}$$

where ω_{cj}^s is the j^{th} natural frequency of sector s with fixed interfaces. $[M^s]$ and $\left[K^{s,0}\right]$ have then the following form

$$\begin{aligned} [M_S^s] &= \left[\begin{array}{ccc} T_{Sr}^\top \, M^s \, T_{Sr}^d & T_{Sr}^\top \, M^s \, T_{Sc}^s & T_{Sr}^\top \, M^s \, T_{Sl}^d \\ T_{Sc}^\top \, M^s \, T_{Sr}^d & I & T_{Sc}^\top \, M^s \, T_{Sl}^d \\ T_{Sl}^\top \, M^s \, T_{Sr}^d & T_{Sl}^\top \, M^s \, T_{Sc}^s & T_{Sl}^\top \, M^s \, T_{Sl}^d \end{array} \right] \\ \left[K_S^{s,0}\right] &= \left[\begin{array}{ccc} T_{Sr}^\top \, K^{s,0} \, T_{Sr}^d & 0 & T_{Sr}^\top \, K^{s,0} \, T_{Sl}^d \\ 0 & \mathcal{K}_{Sc}^s & 0 \\ T_{Sl}^\top \, K^{s,0} \, T_{Sr}^d & 0 & T_{Sl}^\top \, K^{s,0} \, T_{Sl}^d \end{array} \right] \end{aligned} \tag{34}$$

There is no stiffness coupling between the interface modes and the interior modes. The coupling is fully integrated in the non-zero terms of the reduced mass matrix. The matrices displayed in figure 4 are obtained with 2×21 interface modes and 10 interior modes at $\Omega = 0$.

Right and left interface modes are built so that they are matched. This ensures that the intersector continuity condition (9) is equivalent to stating that left generalized DOFs of one sector are equal to right generalized DOFs of the next one:

$$[c_l][T_{Sl}] = [c_r][T_{Sr}] \Longleftrightarrow \{q_{Sl}^s\} = \left\{q_{Sr}^{s+1}\right\} \tag{35}$$

This condition makes the assembly of a disk model with respect to the generalized coordinates really straight forward, leading to block diagonal matrices obtained by the assembly of those of the sector superelements.

With this representation, mistuning is directly taken into account through slight deviations of the natural frequencies of each sector s with fixed interfaces on the diagonal terms of the reduced stiffness:

$$\forall s \in \mathbb{N}_{N_s - 1}, \, [\mathcal{K}_{Sc}^s] = [I + \Delta^s] \left[\mathcal{K}_{Sc}^0\right] \tag{36}$$

$[\Delta^s]$ is a diagonal matrix containing the mistuning factors.

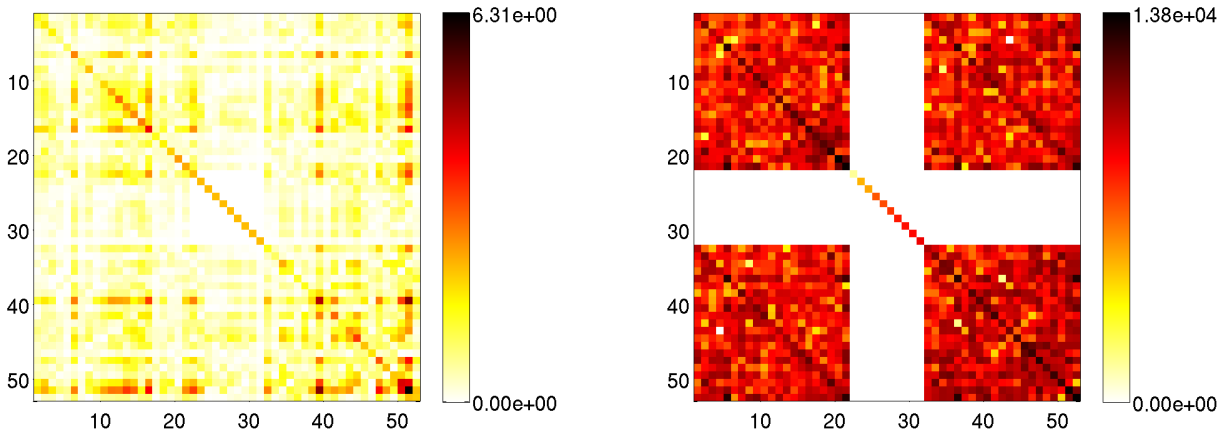

Figure 4: Reduced matrices $[M_S^s]$ and $[K_S^{s,0}]$

3.3 Verification in the case of a tuned disk

Before any consideration of mistuning it was necessary to verify the reduction technique on a tuned disk, in particular to be sure that the modes used to build the reduction basis are obtained exactly with the reduced model. A model of the disk at $\Omega = 0$ was then built using a basis composed of 2×21 interface modes built from 3 single or paired modes with $\delta \in \{0, 3\}$ and a frequency in the range $[1, 5]$ to account for the disk-dominated motion and 10 modes of the sector with fixed interfaces to account for the blade-dominated motion. Table 1 summarizes the number of DOFs of the different models used in this study.

Model	Full FE	QC reduced
Sector	14355	52
Assembled disk	293457	713

Table 1: Number of DOFs of each model

The modes obtained with the reduced problem were compared to the modes given by the cyclic substructuring technique. The resulting graph $\omega_j(\delta)$ and the corresponding frequency relative error for 10 single or paired modes with $\delta \in \{0, 11\}$ in the frequency range $[1, 15]$ are given in figure 5.

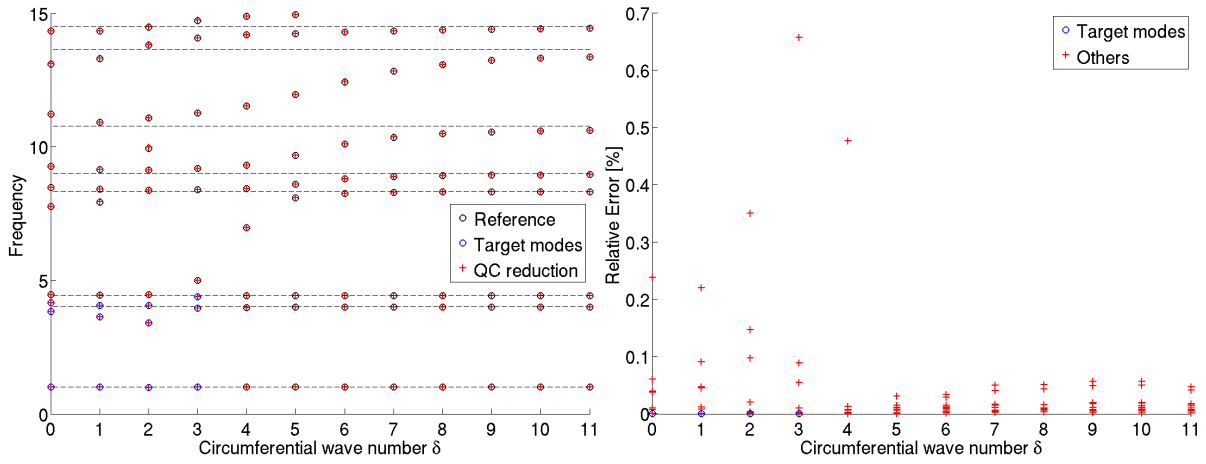

Figure 5: $\omega_j(\delta)$ and frequency relative error for the tuned disk

As expected, this error is zero for the targeted values of δ and stays under 0.7% for the non-target modes in a three times wider frequency band than that of the target modes. One notices that the use of sector modes

with fixed interfaces overstimates by around 0.1% the frequencies of cyclic modes with high values of δ. As the modes are complex conjugate for almost all values of δ, a specific MACM criterion has to be used to check the correlation between reference and reduced modeshapes:

$$MACM_{kl} = \frac{\mathcal{M}(\{\phi_k\},\{\phi_l\})^2}{\mathcal{M}(\{\phi_k\},\{\phi_k\})\mathcal{M}(\{\phi_l\},\{\phi_l\})}$$
$$\text{where } \mathcal{M}(\{U\},\{V\}) = \left|\Re\{U\}^\top[M]\Re\{V\} + \Im\{U\}^\top[M]\Im\{V\}\right| \tag{37}$$

The correlation between the reduced modes and the reference modes computed with the cyclic substructuring is very good. Naturally, the correlation between the target modes and the corresponding reduced modes is excellent as these modes are found exactly with the reduced model. Maximum accuracy is obtained for modes with either small δ at low frequencies or high δ as they are very close to that of the reduction basis.

3.4 Application to mistuning

The sample set of frequencies of the sector with fixed interfaces shown in figure 6 was used to illustrate considerations of mistuning. These frequencies are found in the diagonal of $\left[K_S^0\right]$, reduced elastic stiffness of the whole disk.

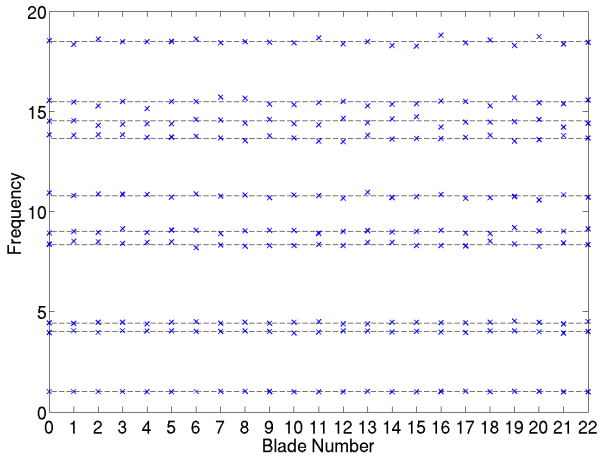

Figure 6: Natural frequencies of the sectors with fixed interfaces

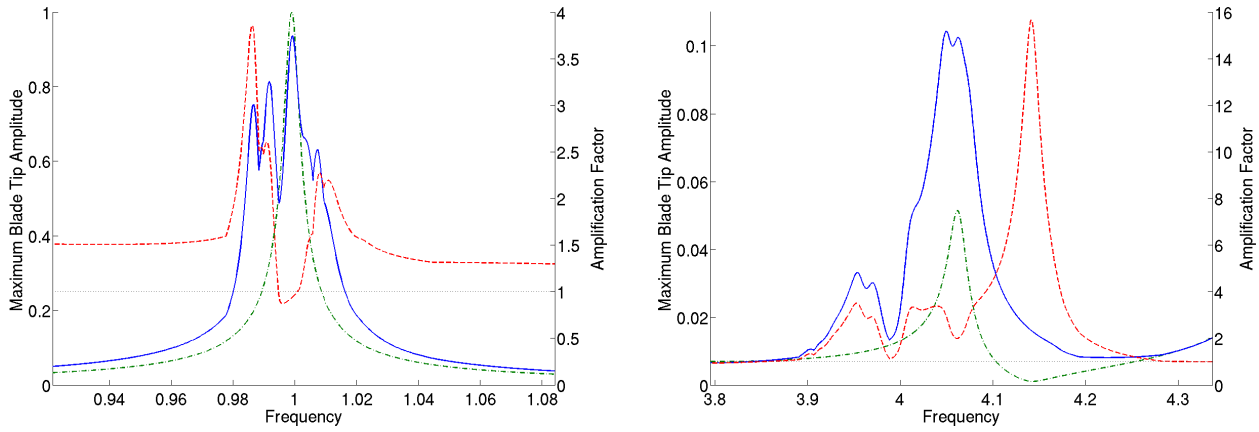

Figure 7: Response to a 1 engine order excitation – · – tuned, — mistuned and – – amplification factor

The forced response of the disk can then be obtained directly from the reduced order model. Figure 7 shows the maximum amplitude of the blade tips for a 1 engine order excitation with a loss factor of 0.005 in the tuned and mistuned cases. The amplification factor is plotted in the same figure. Peak scattering and huge variations of the amplification factor appears clearly in the vicinity of the tuned resonances. As can be seen in this figures, the frequency resolution has to be small to correctly capture frequency scattering and a small but accurate reduced model is mandatory. In this study, the obtained responses use a resolution of 3.10^{-3} with a total of 32768 points of frequency as the minimum difference between the natural frequencies of two different sectors with fixed interfaces is around 5.10^{-3}.

4 Variable speed fixed basis models

Another objective of this study was to accelerate the computation of Campbell diagrams, i.e. diagrams that represents the evolution of the modal frequencies with respect to the rotation speed, in the tuned and mistuned cases.

4.1 Multi-model reduction

Dynamic problems (1) or (11) form parametric families and they can be solved using a multi-model (MM) reduction technique [12]. Their solutions are sought in a subspace generated by some exact solutions targeted at selected values of the parameter, here the rotation speed Ω. One then builds a constant reduction basis whose form is

$$[T_\Omega]_{N\times N_\Omega} = \left[\begin{array}{cccc} [\Phi(\Omega_1)] & [\Phi(\Omega_2)] & \cdots & [\Phi(\Omega_n)] \end{array}\right] \tag{38}$$

$[\Phi(\Omega)]$ are either tuned modes on a single sector or mistuned modes on the whole disk. Target modes can also be defined as a set of modes of interest but this time with respect to the rotation speed. Once more, they would then be found exactly by the resolution of the reduced problem [20].

If one considers the full disk problem (the transposition to the sector problem is easy), the dynamic stiffness is projected onto the subspace generated by $[T_\Omega]$

$$[Z_\Omega]_{N_\Omega\times N_\Omega}\{q_\Omega\}_{N_\Omega\times 1} = \{f_\Omega\}_{N_\Omega\times 1} \tag{39}$$

with

$$[Z_\Omega(\omega,\Omega)] = -\omega^2\,[M_\Omega] + i\,\omega\,[C_\Omega] + \sum_{p=0}^{2}\Omega^{2p}\,\left[K_\Omega^p\right] \tag{40}$$

where $[M_\Omega] = \left[T_\Omega^\top\ M_\Omega\ T_\Omega\right]$, $[C_\Omega] = \left[T_\Omega^\top\ C_\Omega\ T_\Omega\right]$ and $\left[K_\Omega^p\right] = \left[T_\Omega^\top\ K_\Omega^p\ T_\Omega\right]$, $p\in\{0,2\}$. The generalized and physical DOFs are related through the following relation:

$$\{q\}_{N\times 1} = [T_\Omega]_{N\times N_\Omega}\,\{q_\Omega\}_{N_\Omega\times 1} \tag{41}$$

Problem (39) of size $N_\Omega \times N_\Omega$ is then solved for any value of interest of Ω. As the matrix polynomial is quadratic in Ω^2, $n=3$ is necessary to achieve sufficient accuracy.

4.2 Campbell diagram of the tuned disk

The considered tuned bladed disk is that of figure 1 and its Campbell diagrams were computed separately in the speed range $[0,10]$ for each single value of $\delta\in\{0,11\}$. To do so, a parametric multi-model was built with a basis of 10 single or paired modes in the frequency range $[1,15]$ computed with the cyclic substructuring technique at $\Omega\in\{0,5,10\}$ and $\Omega\in\{0,7.5,10\}$. Figure 8 displays the diagram for $\delta=1$ and it is compared to the results obtained with the full sector problem at each speed step. The maximum of the relative error for

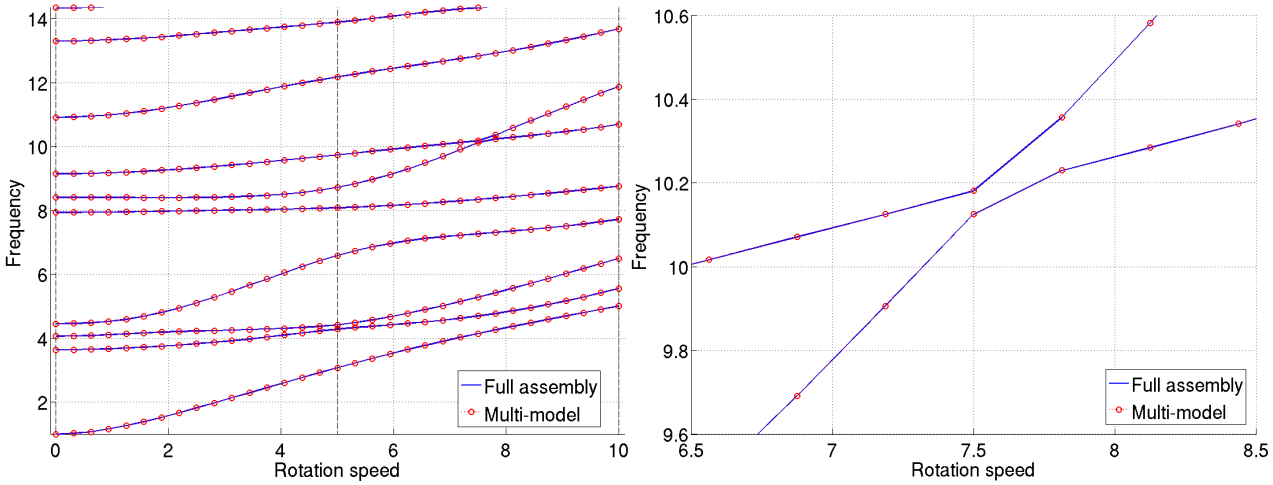

Figure 8: Campbell diagram for $\delta = 1$ and veering region

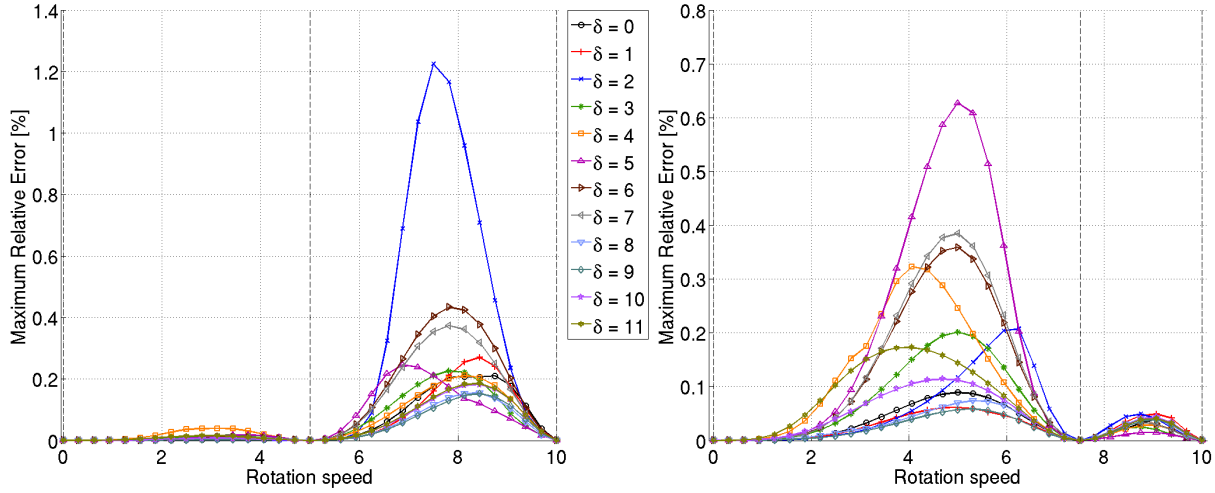

(a) (b)

Figure 9: Maximum frequency error for a multi-model basis at (a) $\Omega \in \{0, 5, 10\}$ – (b) $\Omega \in \{0, 7.5, 10\}$

each of the 10 single or pairs of modes in the frequency range $[1, 15]$ for each value of δ is plotted in figure 9. The vertical dashed lines refer to the target speeds.

The Campbell diagrams are perfectly merged, this is confirmed by the fact that the maximum relative error is under 0.7% except for the 10^{th} pair of modes with $\delta = 2$ in figure 9 (a). This also illustrates the fact that the choice of the speed values to build the basis is the key point: $\Omega = 7.5$ as the intermediate speed increases accuracy as the maximum error in figure 9 (a) is located in the vicinity of this speed. As expected this error is zero for the target modes corresponding to the retained values of Ω in the basis. Moreover, the frequency veering in speed [21] is correctly taken into account by the multi-model as can be seen in figure 8. Besides, the check of the modeshapes is mandatory in those regions and the same MACM criterion is used. Multi-model and reference modes are in fact perfectly correlated for every value of speed in general and around the veering points in particular. All these results show that exact solutions computed at only three rotation speeds are sufficient to estimate the solution at any intermediate speed with great accuracy.

4.3 Multi-level reduction computations

The results of section 3 allow the use of a set of target modes at some selected speeds and with selected values of δ to build the multi-model reduction bases by generating the remaining needed modes with a quasi-cyclic reduced model. These bases can then be used to compute the Campbell diagrams and the forced responses in either tuned or mistuned cases.

In the tuned case it is very close to that of figure 8 and will not be reproduced here for brevity. The maximum relative error is plotted for each speed and each value of δ. The target modes are indeed found exactly by the multi-model as displayed in figure 10 (a) and the error stays below 0.02% in the frequency range of the target modes. Figure 10 (b) also shows that the frequency error is still small, below 1.4%, in a three times wider frequency band. As expected, the frequency error committed on the basis modes due to the quasi-cyclic reduction technique appears directly in this figure and for $\Omega = 0$ it corresponds exactly to the maximum enveloppe of figure 5. The two levels of error that add to each other can thus be clearly seen. The first error is induced by the quasi-cyclic reduction technique as described in section 3.3 and then a second error is superimposed on the previous one by the multi-model approach. Nevertheless, estimations remain sufficiently accurate to be used to predict the vibratory state of rotating tuned or mistuned disks.

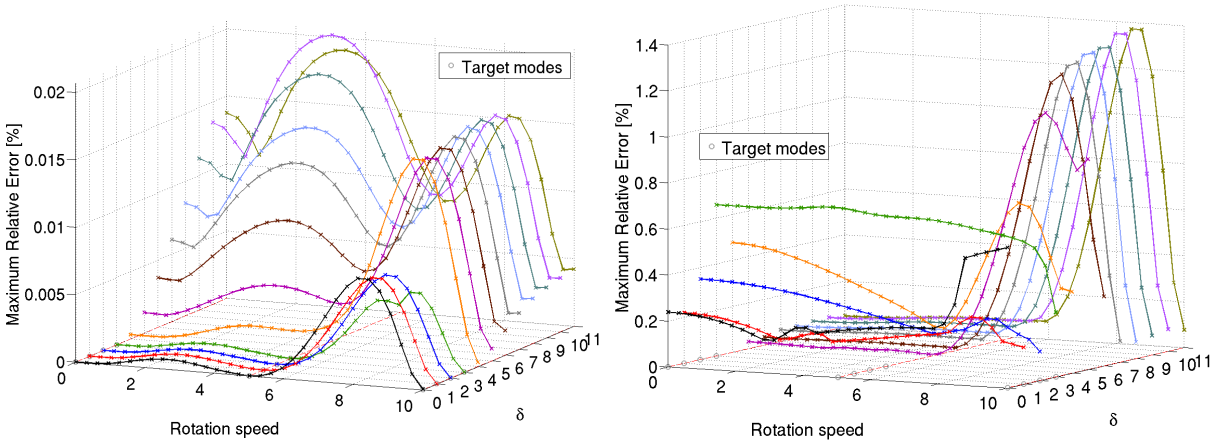

(a) (b)

Figure 10: Maximum frequency error for a multi-model built from a QC disk model in the frequency band (a) $[1, 5]$ – (b) $[1, 15]$

5 Conclusions

The quasi-cyclic reduction technique proposed in this paper aims to build a reduced disk model in which each individual sector is considered as a superelement whose properties can be slightly deviated from the tuned configuration to take mistuning into account. It allows the selection of a target set of modes which are found exactly with the reduced disk model. Other modes are then estimated with an accuracy that is directly related to the choice of target modes. The size of this reduced model is such that forced responses computations are quite fast with a speed that is independent of mistuning level.

The sector reduction technique was then extended to allow fast computations of the Campbell diagrams or forced response at variable speeds. The procedure uses exact cyclic symmetry computations of certain target modes at three rotations speeds to generate the reduced model. The resulting reduced model can then be used to predict modes or forced responses at any speed or mistuning level.

References

[1] M. P. Castanier and C. Pierre. Modeling and Analysis of Mistuned Bladed Disk Vibration: Status and Emerging Directions. *Journal of Propulsion and Power*, 22(2):384–396, 2006.

[2] M.-T. Yang and J. H. Griffin. A Reduced Order Approach for the Vibration of Mistuned Bladed Disks Assemblies. *ASME Journal of Engineering for Gas Turbines and Power*, 119:161–167, 1997.

[3] R. Bladh, M. P. Castanier, and C. Pierre. Component-mode Based Reduced Order Modelling Techniques for Mistuned Bladed Disks – Part I : Theoretical Models. *ASME Journal of Engineering for Gas Turbines and Power*, 123:89–99, 2001.

[4] F. Moyroud, T. Fransson, and G. Jacquet-Richardet. A Comparison of Two Finite Element Reduction Techniques for Mistuned Bladed Disks. *ASME Journal of Engineering for Gas Turbines and Power*, 124:942–952, 2002.

[5] R. Bladh, C. Pierre, M. P. Castanier, and M. J. Kruse. Dynamic Response Prediction for a Mistuned Industrial Turbomachinery Rotor Using Reduced-Order Modeling. *ASME Journal of Engineering for Gas Turbines and Power*, 124:311–324, 2002.

[6] D. M. Tran. Component mode synthesis methods using interface modes. application to structures with cyclic symmetry. *Computers and Structures*, 79:209–222, 2001.

[7] M.-T. Yang and J. H. Griffin. A Reduced Order Model of Mistuning Using a Subset of Nominal System Modes. *ASME Journal of Engineering for Gas Turbines and Power*, 123:893–900, 2001.

[8] D. M. Feiner and J. H. Griffin. A Fundamental Model of Mistuning for a Single Family of Modes. *ASME Journal of Turbomachinery*, 124:597–605, 2002.

[9] E. P. Petrov, K. Y. Sanliturk, and D. J. Ewins. A New Method for Dynamic Analysis of Mistuned Bladed Disks Based on the Exact Relationship Between Tuned and Mistuned Systems. *ASME Journal of Engineering for Gas Turbines and Power*, 124:586–597, 2002.

[10] S. H. Lim, M. P. Castanier, and C. Pierre. Vibration Modeling of Bladed Disks Subject to Geometric Mistuning and Design Changes. *45th AIAA/ASME/ASCE/AHS/ASC Structures, Structural Dynamics and Materials Conference*, 2004.

[11] P. Marugabandhu and J. H. Griffin. A Reduced-Order Model for Evaluating the Effect of Rotational Speed on the Natural Frequencies and Mode Shapes of Blades. *ASME Journal of Engineering for Gas Turbines and Power*, 123:772–776, 2003.

[12] E. Balmes. Parametric families of reduced finite element models. theory and applications. *Mechanical Systems and Signal Processing*, 10(4):381–394, 1996.

[13] SDTools. *Viscoelastic vibration toolbox, User Manual*, 2004.

[14] D. J. Ewins. Vibration characteristics of bladed disk assemblies. *Journal of Mechanical Engineering Science*, 15(3):165–186, 1973.

[15] E. Capiez-Lernout. *Dynamique des structures tournantes a symetrie cyclique en presence d'incertitudes aleatoires. Application au desaccordage des roues aubagees*. PhD thesis, Universit de Marne-La-Valle, 2004.

[16] B. Lalanne and M. Touratier. Aeroelastic vibrations and stability in cyclic symmetric domains. *International Journal of Rotating Machinery*, 6(6):445–452, 2000.

[17] A. V. Srinivasan. Flutter and Resonant Vibration Characteristics of Engine Blades. *ASME Journal of Engineering for Gas Turbines and Power*, 119:742–775, 1997.

[18] D. J. Ewins. The effects of detuning upon the forced vibrations of bladed disks. *Journal of Sound and Vibration*, 9(1):65–79, 1969.

[19] E. Balmes. Use of generalized interface degrees of freedom in component mode synthesis. *International Modal Analysis Conference*, pages 204–210, 1996.

[20] E. Balmes. High modal density, curve veering, localization: a different perspective on the structural response. *Journal of Sound and Vibration*, 161(2):358–363, 1993.

[21] D. Afolabi and O. O. Mehmed. On Curve Veering and Flutter of Rotating Blades. *ASME Journal of Engineering for Gas Turbines and Power*, 116:702–708, 1994.